Design Elements of a Prototype Self-mooring AUV

Robert Briggs*, Brian McCarter†, Wayne L. Neu* and Daniel J. Stilwell†
*Department of Aerospace and Ocean Engineering,
†The Bradley Department of Electrical and Computer Engineering,
Virginia Polytechnic Institute and State University
Blacksburg, VA 24061
{rcbriggs, mccarter, neu, stilwell}@vt.edu

***Abstract*— The Virginia Tech Self-Mooring Autonomous Underwater Vehicle (AUV) is capable of mooring itself on the seafloor for extended periods of time. The AUV is intended to travel to a desired mooring location, moor itself on the seafloor, and then release the mooring and return to a desired egress location. In addition, the AUV is designed to be inexpensive. The self-mooring concept was successfully tested on a small-scale platform known as the Virginia Tech 475 AUV. This report covers the major design elements of the self-mooring AUV, experiments that were conducted to refine the engineering analysis, and the results of successful field trials with this small-scale prototype.**

I. Introduction

For a number of data collection operations, it is desirable to be able to deploy an autonomous underwater vehicle (AUV) which can travel to a predetermined location, station itself in the water column at this location while recording environmental data over an extended time frame and then return to a recovery location. An attempt at developing this capability by designing an AUV which is capable of mooring itself on the seafloor is described below. The mooring system chosen uses a false nose that serves as an anchor. The platform used to develop this capability is the Virginia Tech 475, shown in Figure 1. It is a reliable, small, conventional streamlined AUV which has been previously used for a number of studies [1], [2], [3]. In its base configuration, it is 4.75 inches in diameter, 38 inches long, weighs 18.5 pounds and displaces 18.7 pounds. A motor in the tail drives a single pusher propeller for propulsion. Four individually actuated fin flaps provide control authority. An existing 475 AUV was modified to act as a prototype for the self-mooring AUV. This paper discusses the design and development of the mooring system and the implementation of an enhanced navigation method, as well as results from field tests of the prototype vehicle.

II. General Design Concepts

The concept of operation requires the vehicle to travel to a desired mooring location, periodically surfacing to obtain its location and update its navigation estimates. At the end of this ingress phase, the vehicle must be within a specified circular error probable (CEP) of the target location. The vehicle will then update its position using GPS and release the anchor. A mooring line attached to the anchor pulls the AUV toward the seafloor. The final mooring location is required to be within a rather small specified CEP about the last known location on the surface. At the end of the mooring time the AUV will release the mooring line and return to a desired egress location. Figure 2 shows the intended mission profile.

Fig. 1. Virginia Tech 475 AUV. The external payloads shown mounted below the vehicles were not used in the present work.

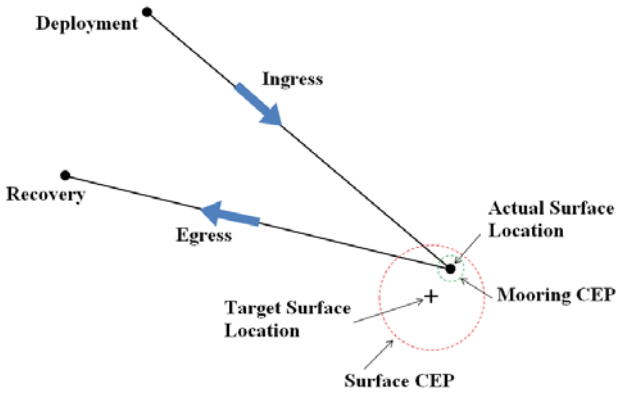

Fig. 2. Schematic of conceptual mooring mission profile.

The design of the mooring system focused on developing a method that would allow the vehicle to quickly descend, would provide a hydrodynamic and balanced vehicle in all configurations, and be reliable through multiple uses and long mission times. As described above, the AUV acquires a GPS location at the surface and then releases the anchor. Since currents may push the AUV away from the specified CEP during descent, the anchor must be designed to allow the AUV to descend very quickly. In addition the AUV should be hydrodynamic with and without the anchor. It was decided that the best way to address these issues was to make the anchor a false nose that attaches to the true AUV nose. Adding

the anchor in this manner lengthens the vehicle, but does not affect the hydrodynamic shape, allowing for an efficient vehicle with the anchor attached. When the anchor is released it will pull the AUV nose down during descent, minimizing drag and increasing the speed of descent. Figure 3 shows the four configurations during the mission. Configurations 1 and 4 will be referred to as the ingress vehicle and the egress vehicle respectively.

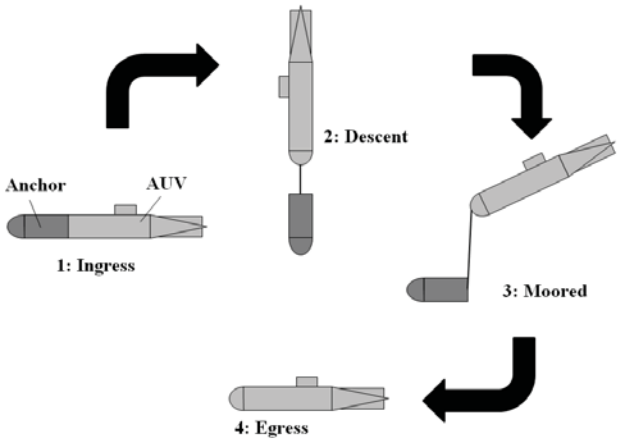

Fig. 3. Four AUV configurations during proposed mission.

A. Anchor Attachment

Two concepts were proposed for attaching the anchor to the nose. One concept was to draw a vacuum inside of the anchor. The pressure differential with the surroundings then forces the anchor to stay on the nose. This concept is simple and requires very little mechanical hardware. The concern with this method is securing the anchor adequately while still having it separate from the seal easily and fall off when released.

The second concept was a mechanically fastened anchor. The anchor would have a threaded rod that protrudes out the back. This rod is inserted into a hole in the nose and through an external-rotor electric motor. By spinning the motor one way it would pull the anchor onto the nose and seal. Turning the motor the other way would push the anchor off. By sizing the threaded rod correctly it can be assured the anchor will break the seal when released.

Due to the simplicity of the system the vacuum attached anchor was chosen. The prototype vehicle described below was outfitted with this system and it proved reliable.

B. Galvanic Release

When the mooring phase of the mission is over the AUV must release the mooring line. This is done with a galvanic release installed on the nose of the AUV, shown in Figure 4. The galvanic release consists of a loop of stainless steel wire (anode), which also serves as the attachment point for the mooring line, and a small stainless steel washer (cathode). If a properly polarized voltage difference is applied between the anode and the cathode while the vehicle is in salt water the resulting current will rapidly corrode the loop of wire. After approximately ten minutes the wire will break and the vehicle will be released from the anchor. This method of release proved to be simple and robust.

Fig. 4. Prototype nose showing galvanic release and vacuum ports.

III. Anchor Design

Since there is no requirement to moor the AUV in a region of strong bottom currents, the grip of the anchor on the bottom was not a concern. Rather, the anchor size was determined by setting the terminal velocity of the anchor-vehicle system during descent. Figure 5 shows the descent profile for a case where the current is split into two separate values. From the surface to a depth of d_1, the current is equal to $v_{cur,1}$. From d_1 to depth d_2, at the seafloor, the current is $v_{cur,2}$. As the vehicle dives the currents will push it away from the surface location, shown by the solid line in Figure 5. The vertical velocity of the AUV must be sufficient that it will reach the seafloor in no more time than it takes it to travel laterally a distance equal to the CEP radius, R. This vertical velocity is the required terminal velocity, approximated by Equation 1. For anchor sizing the worst case scenario, where the currents are at their maximum values and are acting in the same direction, is considered. If the vehicle is assume to reach its terminal velocity immediately upon beginning its descent, a consideration of travel times yields,

$$v_{terminal} = \frac{v_{cur,1} d_1 + v_{cur,2} \left(d_2 - d_1\right)}{R} \tag{1}$$

Since the submerged weight of the anchor is much greater than that of the submerged egress vehicle it can be assumed that during the descent the two bodies are separated by a few meters (the length of the mooring line), enabling the drag of each body to be treated separately. The anchor is shaped like a cylinder with a half sphere front and blunt back, shown in Figure 6. This shape has a coefficient of drag, $C_{d,anchor}$, which is very nearly 0.2 for fineness ratios between 2 and 10 [4]. The reference area for this drag coefficient is the cross-sectional area, $A = \pi r^2$. Thus the drag on the anchor is,

$$F_{d,anchor} = \frac{1}{2} \rho v^2 A C_{d,anchor} \tag{2}$$

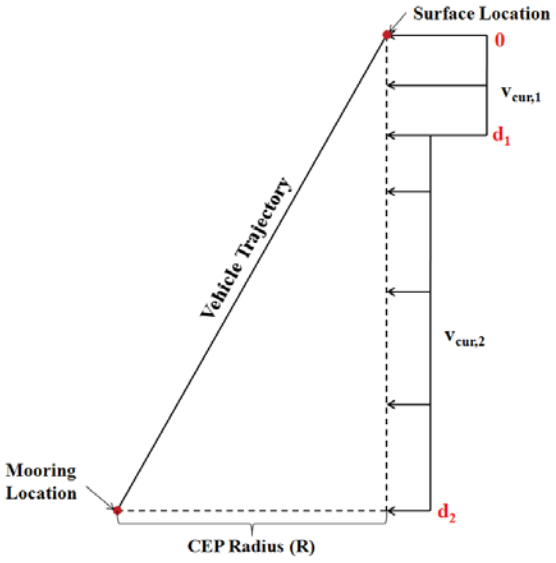

Fig. 5. Sketch of side drift during descent for a two current case.

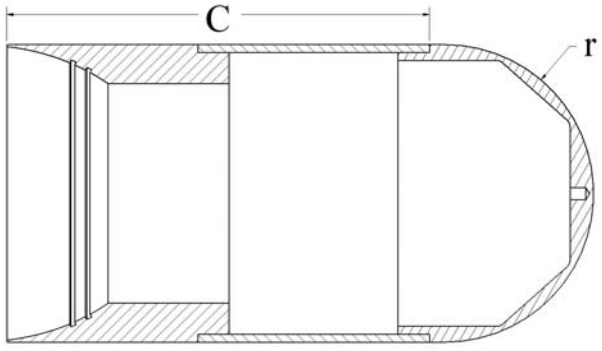

Fig. 6. Prototype Anchor Shape

where ρ is the water density.

The drag on the AUV ($F_{d,vehicle}$) is separated into two parts: the main body and the sail. The body drag is calculated by the corrected form factor approach [4]. First the coefficient of friction, $C_{f,body}$, is calculated as a function of velocity, v, body length, ℓ, and the kinematic viscosity of water, ν. The friction coefficient used is the 1957 ITTC line [5].

$$Re_\ell = \frac{v\ell}{\nu} \tag{3}$$

$$C_{f,body} = \frac{0.075}{\left(\log_{10} Re_\ell - 2.0\right)^2} \tag{4}$$

An appropriate form factor is chosen for the vehicle's shape. Since the prototype will be a modified 475 vehicle, the chosen form factor is a cylinder with hemispherical ends. The form factor, FF, is a function of body length, ℓ, and diameter, d.

$$FF = 2.643 + 1.5\left(\frac{d}{\ell}\right)^{1.5} + 7\left(\frac{d}{\ell}\right)^{3} \tag{5}$$

The coefficient of drag, $C_{d,body}$, is obtained by multiplying the coefficient of friction, $C_{f,body}$, by the form factor, FF, and, since the reference area for the coefficient of friction is the total wetted surface area, S_{wet}, and that for the coefficient of drag is the cross-sectional area, A, the ratio of these areas.

$$C_{d,body} = C_f \frac{S_{wet}}{A} FF \tag{6}$$

Further employing the shape approximation of a cylinder with hemispherical ends, the area ratio is reduced to

$$\frac{S_{wet}}{A} = 4\frac{\ell}{d} \tag{7}$$

The drag force on the body is then

$$F_{d,body} = \frac{1}{2}\rho v^2 A C_{d,body} \tag{8}$$

The sail drag is calculated by the general airfoil approach [4]. The coefficient of friction, $C_{f,sail}$, is calculated as in (4), except the Reynolds number, Re_c, is referenced to the airfoil chord, c.

$$Re_c = \frac{vc}{\nu} \tag{9}$$

$$C_{f,sail} = \frac{0.075}{\left(\log_{10} Re_c - 2.0\right)^2} \tag{10}$$

The coefficient of drag, $C_{d,sail}$ is obtained by multiplying $C_{f,sail}$ by a ratio of areas which can be approximated as a function of c and airfoil thickness, t [4]. The drag on the sail is calculated as in (8) by using $A = cb$, where b is airfoil span.

$$C_{d,sail} = 2\left[1 + 2\frac{t}{c} + 60\left(\frac{t}{c}\right)^4\right] C_{f,sail} \tag{11}$$

$$F_{d,sail} = \frac{1}{2}\rho v^2 \left(cb\right) C_{d,sail} \tag{12}$$

The total drag on the vehicle is estimated as the sum of (8) and (12). The resulting drag is increased by 25% to account for the drag of the fins and transducer. This was empirically determined from previous experiments with the 475 vehicle and is felt to be conservative for the prototype vehicle.

$$F_{d,vehicle} = \left(F_{d,body} + F_{d,sail}\right) \times 1.25 \tag{13}$$

The total drag of the two body, anchor-vehicle system is just the sum of the anchor and vehicle drags.

$$F_d = F_{d,vehicle} + F_{d,anchor} \tag{14}$$

At terminal velocity during descent, the wet weight of the anchor, $W_{a,wet}$, defined as the net weight of the flooded anchor removed from the egress vehicle, must equal the total drag, F_d, of the descending two body system.

$$W_{a,wet} = F_d \tag{15}$$

Also, for a properly ballasted ingress vehicle, the dry weight, $W_{a,dry}$, defined as the weight of the unflooded anchor when attached to the egress vehicle or the weight of the ingress vehicle minus the weight of the egress vehicle, must equal the weight of the additional water displaced by the ingress vehicle over that displaced by the egress vehicle. The volume of this additional displacement is equal to the volume of the anchor

minus the volume, V_{lost}, occupied by the portion of the egress vehicle's nose that extends into the anchor when it is attached to the egress vehicle. Referring to Figure 6, this additional displacement can be written as

$$\nabla_{anchor} = \frac{2}{3}\pi r^3 + C\pi r^2 - V_{lost} \tag{16}$$

Thus,

$$W_{a,dry} = \rho \nabla_{anchor} \tag{17}$$

Further, for proper trim, the longitudinal center of gravity (LCG) must coincide with the longitudinal center of buoyancy (LCB) for both the egress and ingress vehicles. Assuming the egress vehicle is properly trimmed, the addition of the anchor must shift the LCG and LCB by equal amounts. This means that the LCG of the anchor mass must coincide with the center of volume of the additional displacement, ∇_{anchor}. Further, if the anchor is to fall vertically during descent, its center of gravity must be located on its axis of rotation.

Proper anchor design then requires adjustment of the length, C, and the anchor mass distribution to simultaneously satisfy Equations 15 and 17 as well as proper placement of the anchor's center of gravity.

For the prototype vehicle, the descent CEP requirement was set to 75 feet at a depth of 100 feet. This gave the size, weight and desired CG location of the anchor. To achieve the proper CG location while keeping manufacturing as simple as possible, the anchor was split into three parts, a machined front and back, and a polycarbonate tube for a center. The anchor front was machined out of steel and the back out of aluminum. The three sections were joined together using silicon sealant. To seal the anchor to the nose of the AUV, the back of the anchor was machined to match the outside contour of the nose. Two o-ring grooves were added to this surface and provided a positive seal.

As a balancing aid, a brass weight ring was added to the anchor. The weight ring was held in the anchor by four thumb screws allowing for easy adjustment fore and aft.

For the mooring line that connects the anchor to the galvanic release, Spectra® line was chosen. A small line was needed so winding it inside the anchor would not require much room, and Spectra® offers a great strength to size ratio. The line was wrapped around a plastic cylinder and secured with candle wax. The cylinder was then mounted in the front inside of the anchor. When the anchor is deployed the wax seal breaks and the line unravels until taut. After initial testing it was found that this securing method deploys well, but for stability of the anchor during descent, a three point bridle was added which connects the mooring line well above the CG of the anchor.

Figure 7 shows the prototype anchor and its design features.

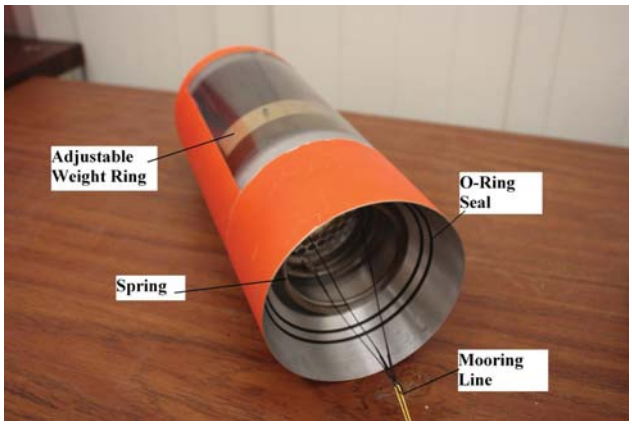

Fig. 7. Prototype Anchor

IV. Navigation

Due to the size, energy requirement and cost the vehicle is not equipped with an inertial measurement unit (IMU) or Doppler velocity log (DVL). Navigation may then be performed by dead reckoning, where vehicle velocity is integrated to estimate position. The self-mooring AUV uses a dead reckoning strategy based on periodic GPS fixes with variable leg lengths. A velocity error model is used as described below.

A. Model

An AUV is given the task of traversing a straight line path in open ocean. It is equipped with attitude and water-relative velocity sensors. The water-relative velocity is less than certain as it is inferred from the measured rate of revolution of the propeller shaft. The vehicle travels along a series of trajectories ℓ_i, traveling for some distance then surfacing for a GPS fix. It begins at position x_0 and travels at a fixed heading and water-relative velocity. At every step i, the AUV proceeds to the next position by the following algorithm:

1) Calculate nominal trajectory ℓ'_i:

$$\hat{\ell}'_i = \frac{x_f - x_{i-1}}{\|x_f - x_{i-1}\|} \tag{18}$$

$$d_i = \min\left\{\|x_f - x_{i-1}\|, d_{max}\right\} \tag{19}$$

$$\ell'_i = d_i \hat{\ell}'_i \tag{20}$$

2) Calculate adjusted trajectory ℓ^*_i with error compensation, and adjusted destination x^*_i:

$$e_{i-1} = x_{i-1} - x'_{i-1} \tag{21}$$

$$\ell^*_i = \ell'_i - e_{i-1} \tag{22}$$

$$x^*_i = x_{i-1} + \ell^*_i \tag{23}$$

3) Execute a course to x^*_i, during which GPS is unavailable.
4) Surface at point x_i, and repeat until $\|x_f - x_i\|$ is less than a radial boundary r_x around the final destination.

The error e_i is measured with GPS at each surfacing, and is assumed to be accurate relative to the distance traveled. The AUV is also assumed to be equipped with an accurate clock. Therefore it is reasonable to model the position error as the integral of a velocity error v_i over the leg time t_i. Velocity error is composed of two components:

- measurable error, e.g. ocean current and sensor mis-calibration.

- unmeasurable error, e.g. local turbulence and integral drift.

We will treat the velocity error as a random variable that is sampled once per leg, drawn from the bivariate normal distribution

$$v_i \sim N(\bar{v}_i, \Sigma_v) \tag{24}$$

where $\bar{v}_i$ is the expected two-dimensional velocity error over that leg (i.e. from a NOAA current model) and Σ_v is the velocity error covariance.

B. Simulation

A monte-carlo simulation demonstrates the effect of varying d_{max}, the maximum distance traveled per leg. The cost, c, of each d_{max} is calculated as

$$c = \frac{t_f - t_{nom}}{t_{nom}} \tag{25}$$

where t_f is the simulated time to transit from x_0 to x_f and t_{nom} is the nominal transit time, as if $\Sigma_v = 0$. Each surfacing event is penalized with a fixed time cost, which simulates the time required to surface, gather GPS data, and dive again. In this simulation, the cost to surface is 90 seconds.

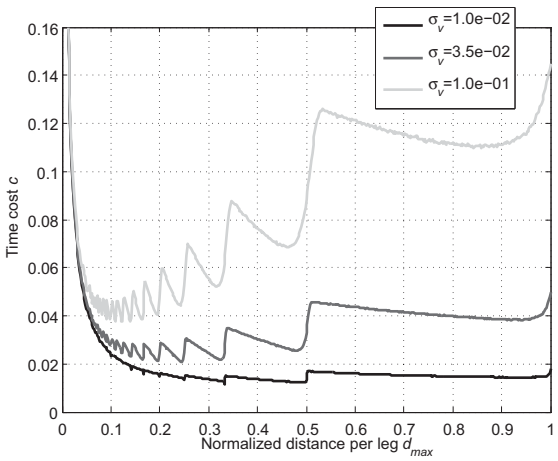

Fig. 8. Navigation cost, c, as a function of max leg length, d_{max}, with varying velocity error covariance, σ_v

The simulation result is given in Figure 8. Here, the velocity error covariance is assumed to be symmetric with form

$$\Sigma_v = \begin{bmatrix} \sigma_v^2 & 0 \\ 0 & \sigma_v^2 \end{bmatrix} \tag{26}$$

The simulation shows cost as a function of maximum leg length for three values of velocity error covariance. There are local cost 'critical points' at locations where d_{max} takes the form

$$d_{max} = 1/a, \quad a \in \mathbb{Z} \tag{27}$$

Note that cost is lower for leg lengths slightly shorter than these critical values, and higher for leg lengths slightly longer. The global minimum for each σ_v curve is driven by the surface cost penalty. For example, the costs for small values of d_{max} are very high because the total cost is then dominated by surface events.

The middle value of velocity error covariance where $\sigma_v = 0.035\ m/s$ is an estimate taken from field work in a typical operating environment. The higher and lower values are chosen to provide insight into how cost is affected by changing conditions.

This result serves as a basis for choosing d_{max} more intelligently than by trial and error. For the case where $\sigma_v = 0.035\ m/s$, the minimum practical cost is estimated to be about 2.1% of the nominal travel time. That means a transit of 4 nautical miles with a nominal travel time of 60 minutes will take 61.3 minutes in the best case. Compare that result to the naive choice of trying to hit the destination in 1 leg (e.g. $d_{max} = 1$) where the cost is 5.0% and actual travel time is 63.0 minutes. Operating environments with greater uncertainty benefit more from this approach than do well known operating environments.

V. Prototype Vehicle

To validate the decisions made during conceptual design a prototype vehicle was constructed (Figure 9). An existing 475 vehicle was modified with expanded payload capacity, an external anchor, galvanic release, and the necessary plumbing (discussed below) to deploy the anchor. Once constructed the prototype vehicle was tested in several phases to prove the various concepts and assumptions made in the design of the self-mooring AUV. First the proper balance between ingress and egress configurations was checked, then the diving capabilities were proven, and finally a full system test was completed.

A. Nose Modifications

The 475 nose needed to be modified to accommodate both a galvanic release and the vacuum system required for attaching and releasing the anchor. A 1/2"' NPT threaded hole was added to the front of the nose to accommodate a galvanic release made from a PVC plug. The vacuum system relied on a servo actuated valve used for hobby aircraft. This valve was placed inside the nose and connected to an extra pressure port placed on the front of the nose, above the NPT hole. The other side of the valve was connected to a quick-connect tube fitting placed on the top of the nose. This allowed a vacuum to be pulled in the anchor via the quick-connect fitting. Once a vacuum was established the valve was closed. When releasing the anchor the valve was open, pulling air and/or water in from outside the vehicle and releasing the vacuum.

Early anchor dive testing proved this method was not sufficient. It was found that the valve restricted the flow into the anchor causing the vehicle to sit in place for over a minute waiting for the anchor to fall off. This would allow the vehicle too much time to drift off target. In addition if the anchor pulls in water and becomes heavy the vehicle could start sinking before the anchor was released. This could result in

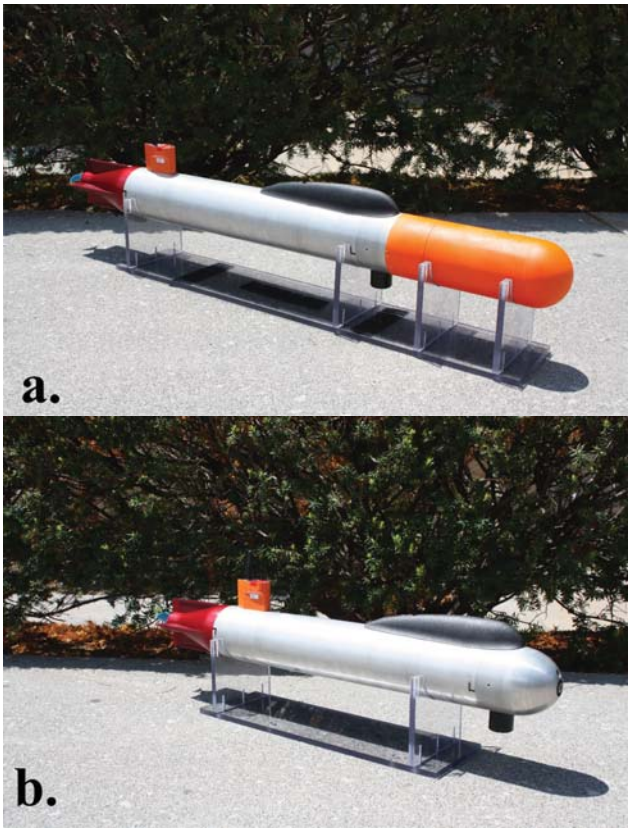

Fig. 9. Prototype self-mooring AUV in both ingress (a) and egress (b) configurations.

the vehicle gliding horizontally a significant distance before the anchor released. To reduce the anchor release time on the surface, it was decided to increase the diameter of the tubing and valve forming the vacuum system. In addition, a carbon dioxide canister was connected to the exterior vacuum port with flexible tubing. The vacuum release could now be accomplished quickly and without weight change by discharging the compressed CO_2 into the anchor.

To accomplish this modification, a new nose was designed. The new nose exterior was the same as the old nose, however by changing the interior a larger valve could be used. The new valve was a regular 2-way valve modified to be driven by a hobby servo, shown in Figure 10. This allowed a much higher flow rate into the anchor. Also the galvanic release was redesigned to be inserted from the front of the nose and seal using an o-ring. This simplified the process of preparing the sub for use and provided a more reliable seal. Since the CO_2 canister connected to the outside of the vehicle a fairing was designed to cover it.

B. Payload Integration

To expand the payload capacity for the expected addition of environmental sensors, the tube of the 475 vehicle was extended by six inches for the prototype. The payload was added forward in the vehicle between the new nose and the vehicle electronics chassis. Placing a payload such that the center of gravity of the payload and any required ballast is in line with the center of buoyancy of the six inch extension will keep the AUV balanced.

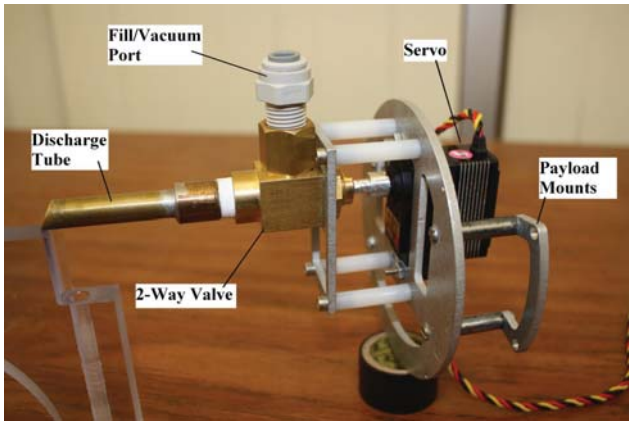

Fig. 10. Internal components of the prototype vacuum system.

VI. Testing

A. Dive Testing

The dive testing was done at depths of 30 feet and 60 feet. The testing helped to validate the anchor sizing and release. Experimental measurements of terminal velocity and time to descend are presented in Table I and Figure 11 along with results from simulations of these events used to validate the model developed. The model used for the simulations did not treat the time between the initialization of the anchor release and the mooring line becoming taut. During this time, the egress vehicle loitered near the surface as the mooring line deployed. This process is shown in Figure 12. The simulation times were shifted to correspond to the time that the mooring line first pulled the vehicle into its rapid descent during the test. The terminal velocity seen in testing was found to be slightly lower than the simulated terminal velocity however the time to descend was more accurately predicted. The velocity discrepancies may be due to variations in the angle of the AUV during the initial portion of the descent or an underestimate of the total drag of the system.

The small dip at the beginning of the actual descent seen in Figure 11 is where the mooring line is unwinding from the anchor. Note the shift in the simulated trajectory to account for this unmodeled phenomenon as discussed above. At the end of the dive the anchor impacts the seafloor, but the AUV continues down. The drag and the buoyancy of the AUV stop it before it reaches the seafloor and then it rises to the mooring height, determined by the length of the mooring line. The length of the mooring line must be long enough that the vehicle has enough distance to stop, before impacting the seafloor. The AUV fully at rest in the moored configuration is shown in Figure 13.

B. Full Systems Test

A full system test was performed twice in the Chesepeake Bay. Both tests were identical. The vehicle was set to have an

TABLE I
SIMULATED VS. ACTUAL DESCENT RESULTS

	Depth	Terminal Velocity		Time to Descend	
		Simulated	*Actual*	*Simulated*	*Actual*
Test 1	30 ft.	1.62 m/s	1.25 m/s	10.3 s	9.8 s
Test 2	30 ft.	1.62 m/s	1.2 m/s	11 s	10.8 s
Test 3	60 ft.	1.63 m/s	1.3 m/s	14.8 s	15.6 s

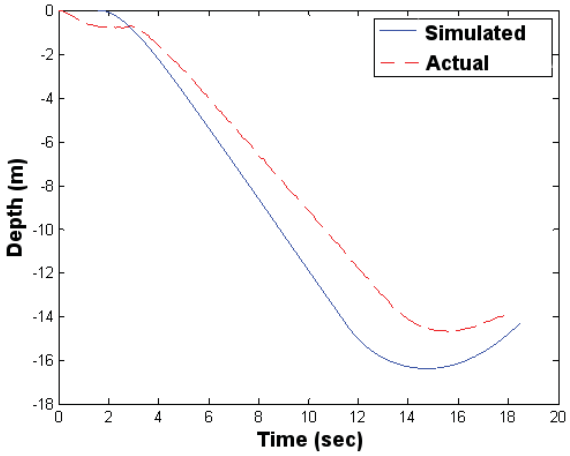

Fig. 11. Simulated vs. actual descent during the 60 ft. dive test.

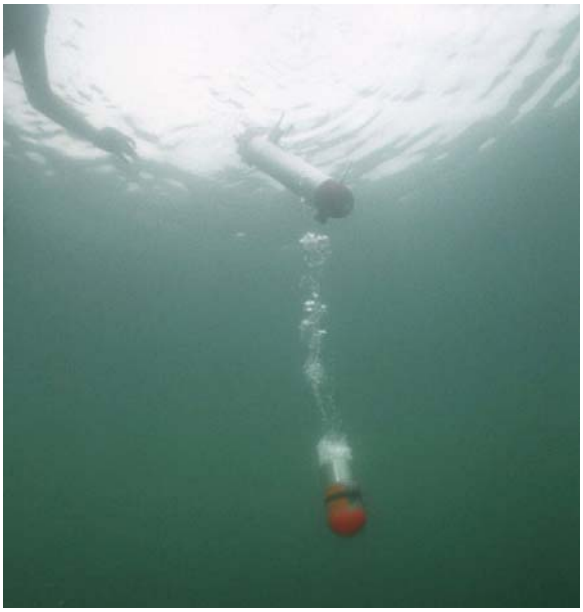

Fig. 12. Initial deployment of mooring line shortly after anchor release during dive testing.

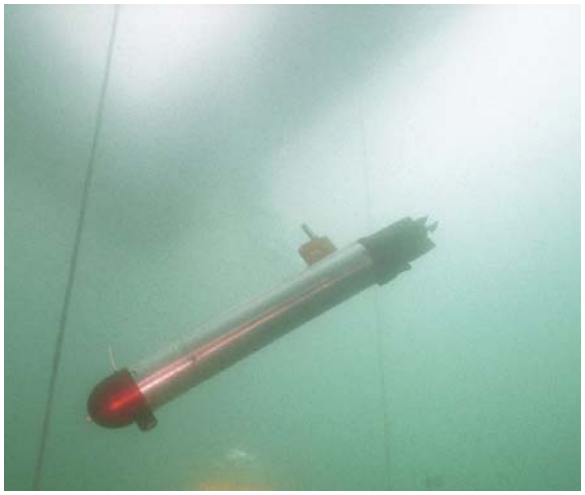

Fig. 13. AUV in the moored configuration during dive testing.

ingress and egress distance of 1600 meters (1 statute mile). The distance between GPS updates was set to be no more than 350 meters. Figure 14 shows the navigation log from the test. The AUV arrived within the CEP at the specified mooring location for both tests. The anchor was then released and the vehicle moored at a depth of 40 feet. After 20 minutes the galvanic release was triggered and the AUV ascended and began the egress phase.

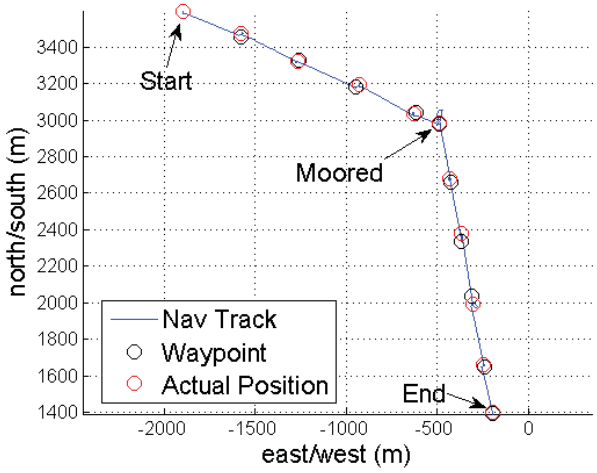

Fig. 14. Navigation track from full system test.

VII. CONCLUSION

The design of a self-mooring AUV was performed and a prototype was constructed as a modification of the Virginia Tech 475 vehicle. The concept employed uses a false nose attached to the AUV as an anchor. The anchor is attached using a vacuum pulled on the volume it encloses. The AUV travels with anchor attached from a deployment point to the desired mooring location. Effective release of the anchor required a rapid relaxation of the vacuum which was accomplished by

allowing compressed gas to escape into the anchor's enclosed volume. This volume then floods, the anchor becomes negatively buoyant and pulls the AUV to its mooring point on the seafloor. At the end of the deployment period, a galvanic release disconnects the mooring line from the AUV and it is free to travel to a recovery point.

In order to limit the cost of the system, the navigation sensors installed on the vehicle were limited and the vehicle navigates using dead reckoning between periodic GPS position measurements. A navigation algorithm was developed which allows the vehicle to recognize and account for velocity errors from current induced drift and sensor errors. A scheme for determining an optimum choice of leg length between surfacings for GPS measurements during lengthy transits was developed and implemented.

A number of tests were conducted to validate the design. Both dive and full system tests showed that the prototype vehicle with mooring system performed as intended. The navigation script proved to be effective for 1.6 km ingress and egress transits. The capability developed during this effort is now available for incorporation into a larger, deep-water capable vehicle.

ACKNOWLEDGMENT

The authors would like to thank Chris Bright, Richard Duelley and Tim Pratt for their help in developing and testing the self-mooring AUV prototype.

REFERENCES

[1] Gadre, A.S., D.K. Maczka, D. Spinello, B.R. McCarter, D.J. Stilwell, W.L. Neu, M.J. Roan, J.B. Hennage. Cooperative localization of an acoustic source using towed hydrophone arrays, in *Proc. IEEE Workshop on Autonomous Underwater Vehicles*, Woods Hole, MA, 2008.

[2] Petrich, J., W.L. Neu, and D.J. Stilwell. Identification of a simplified AUV pitch axis model for control design: Theory and experiments. In *OCEANS 2007, Proceedings of MTS/IEEE*, Vancover, BC, Canada, 2007.

[3] Petrich, J., and D.J. Stilwell. Model simplification for AUV pitch-axis control design, in *Journal of Ocean Engineering*, 37(7): 638652, 2010.

[4] Hoerner, S.F., *Fluid-Dynamic Drag*, Hoerner Fluid Dynamics, Bakersfield, CA, 1992.

[5] ITTC (1957), Proc. 8th ITTC, Madrid, Spain, published by Canal de Experiencias Hidrodinamicas, El Pardo, Madrid.